LAWRENCE
LIVERMORE
NATIONAL
LABORATORY

LLNL-PROC-431291

EXPERIMENTAL TESTS OF VANADIUM STRENGTH MODELS AT HIGH PRESSURES AND STRAIN RATES

H. Park, N. R. Barton, R. C. Becker, J. V. Bernier, R. M. Cavallo, K. T. Lorenz, S. M. Pollaine, B. A. Remington, R. E. Rudd

May 11, 2010

1st TMS-ABM International Materials Congress Conference
Rio de Janeiro, Brazil
July 26, 2010 through July 30, 2010

Disclaimer

EXPERIMENTAL TESTS OF VANADIUM STRENGTH MODELS AT HIGH PRESSURES AND STRAIN RATES

Hye-Sook Park, N.R. Barton, R. C. Becker, J. V. Bernier, R. M. Cavallo,
K.T. Lorenz, S. M. Pollaine, B. A. Remington, and R. E. Rudd

Lawrence Livermore National Laboratory, Livermore, CA 94550 USA

Abstract

Experimental results showing significant reductions from classical in the Rayleigh-Taylor (RT) instability growth rate due to high pressure material strength or effective lattice viscosity in metal foils are presented. On the Omega Laser in the Laboratory for Laser Energetics, University of Rochester, target samples of polycrystalline vanadium are compressed and accelerated quasi-isentropically at ~1 Mbar pressures, while maintaining the samples in the solid-state. Comparison of the results with constitutive models for solid state strength under these conditions show that the measured RT growth is substantially lower than predictions using existing models that work well at low pressures and long time scales. High pressure, high strain rate data can be explained by the enhanced strength due to a phonon drag mechanism, creating a high effective lattice viscosity.

I. INTRODUCTION

Studying material properties under compression at high pressure is a new frontier in material science[1]. Macroscopically, materials deformed under compression can change their yield strength, tensile strength, ductility, toughness and work hardening. Understanding these mechanisms allow material engineers to tailor the mechanical properties of materials to suit a variety of different applications. Microscopically, deformation under compression changes the atomic lattice arrangement of a material. The lattice structure can also undergo phase transitions when subjected to high pressure and temperature.[2] This microscopic change in the lattice structure can have a significant impact on the macroscopic properties of a material. A common method of loading materials to high pressure is the use of shocks. Shock loading, however, causes heating, potentially melting the material, thus preventing study of lattice properties at high pressure and high density in the solid state. A way to load materials to high pressure under nearly isentropic conditions is by ramp compression.[1,3,4] One approach to ramp loading is to use a laser to drive a strong shock through a low-Z reservoir, which unloads as a rarified plasma across a vacuum gap that ten stagnates on the sample. This creates a nearly isentropic pressure profile in the sample.

Utilizing this reservoir-gap configuration, our observational parameter to study material dynamics under extreme conditions is Rayleigh-Taylor instability (RTI). When a low density fluid of density ρ_L accelerates a higher density fluid of density ρ_H, conditions for the buoyancy driven Rayleigh-Taylor instability are set up.[5,6] Perturbations at the interface can grow, generating “bubbles” of the lower density fluid rising into the denser fluid, and “spikes” of the latter sinking through the low density fluid.[7] We present experimental and simulation results that demonstrate an RT instability stabilization mechanism at high pressure, namely, effective lattice viscosity via a phonon drag mechanism. This high pressure stabilization mechanism is

predicted to increase with pressure, provided the solid-state lattice is maintained. Studying material strength properties using RTI was first utilized in the J. F. Barnes' experiment where a rippled Al plate was accelerated by high explosives reaching about 100 kbar peak pressure.[8] Analytic theory for RTI in solids has also been developed.[9] This paper presents laser driven experimental results reaching about 900 kbar peak pressure in solid state samples of vanadium (V), a body-centered cubic (BCC) metal.[10]

The fundamental carriers of deformation in a solid-state sample are dislocations. The resistance to dislocation transport is the microscopic basis for material strength. Dislocations move in discrete step sizes, *b*, called a Burgers vector, of order the crystal lattice spacing. When large numbers of dislocations, of order ~10^4, move in concert, macroscopic deformation occurs. Generally, dislocations in a solid exist prior to loading, and are pinned against barriers, such as the Peierls barrier in BCC metals. When a shear stress is applied, in our experiments by the laser created ramp drive, dislocations may remain pinned or jump over the barrier depending on the height and extent of the barrier and the magnitude of the applied shear stress. There are two relevant mechanisms by which the dislocations can overcome the barrier at the high pressures and strain rates studied here: thermal activation and phonon drag. For low strain rates, thermal fluctuations in the lattice can kick the dislocation over the barrier, after which it will glide along a glide plane in the lattice till it gets pinned (stopped) at another barrier. This mechanism of deformation is called thermal activation. If the applied shear stress is sufficiently strong, however, the dislocations can be pushed over the tops of all barriers. In this case, the resistance to the dislocation motion can come from scattering of lattice phonons and is referred to as phonon drag. In the thermal activation regime, the dislocation velocity increases exponentially with an increasing shear stress, whereas in the phonon drag regime, the increase of velocity with shear stress is linear.

The starting point in constructing a strength model is Orowan's equation,[11,12] $\dot{\varepsilon} = \rho_{disloc} b \bar{v}_{disloc}$, where ε is plastic strain (such as a change in rippled amplitude, $\Delta\eta$, due to the RT instability, normalized by the rippled wavelength, $\varepsilon \sim \Delta\eta/\lambda$), $d\varepsilon/dt$ is strain rate, ρ_{disloc} is mobile dislocation density, *b* is the Burgers vector, and $\langle v_{disloc} \rangle$ is the average dislocation velocity. Relationships for average dislocation velocity in the thermal activation regime and phonon drag regime are inserted into Orowan's equation. Two popular models that result are the Steinberg-Lund model,[13] and the Preston-Tonks-Wallace or PTW model.[14] The Preston-Tonks-Wallace (PTW) strength model is strain rate dependent, and is based on the deformation mechanisms of thermal activation for low strain rates (which assumes dislocations are pinned against stress barriers in the lattice and require a thermal "kick" to surmount the barrier and glide to the next pinning site) and viscous phonon drag for high strain rates (which assumes dislocations are gliding over the tops of stress barriers, resisted only by the drag from scattering of lattice phonons). The PTW strength in the low-strain limit is expressed as:

$$\sigma_y = 2G \max\left\{ y_0 - (y_0 - y_\infty)\mathrm{erf}[\kappa \hat{T} \ln(\gamma\dot{\xi}/\dot{\varepsilon})],\ s_0(\dot{\varepsilon}/\gamma\dot{\xi})^{\beta} \right\}, \qquad (1)$$

where $G = G(P,T)$ is the pressure dependent shear modulus, erf is the mathematical error function, $\dot{\varepsilon}$ is the strain rate, $\hat{T}$ is the normalized temperature, $T_{melt}(\rho)$ is the Lindeman law melt temperature,[15,16] $\dot{\xi}$ is a reference inverse time scale, $\gamma\dot{\xi} = \dot{\varepsilon}_{crit}$ is the critical strain rate above which the deformation switches from thermal activation to phonon drag, and y_0, y_∞, κ, γ, s_0, and β are material dependent input parameters. These parameters roughly correspond

material properties according to $\gamma \sim \rho_{disloc} b^2$, $\kappa \sim 1/U_k$, $y_\infty \sim \sigma_A$, $y_0 \sim \sigma_A + \sigma_P$, and y_0-$y_\infty \sim \sigma_P$, where ρ_{disloc}, b, U_k, σ_A, and σ_P represent dislocation density, Burgers vector, kink activation energy, athermal strength component, and Peierls stress, respectively.[17] The PTW strength, σ_s, in the high-strain (saturated) limit has a similar form, only with s_0 and s_∞ replacing y_0 and y_∞. These are combined in a Voce work hardening prescription for arbitrary strain, ε.[14] We will also show comparisons to an older model, the Steinberg-Guinan model,[16] which is written as, $\sigma = \sigma_0 f(\varepsilon) G/G_0$, where $f(\varepsilon) = [1 + \beta(\varepsilon_i + \varepsilon)]^n$, and

$$G = G_0 \left[1 + \left(\frac{G_P'}{G_0} \right) \frac{P}{\eta^{1/3}} + \left(\frac{G_T'}{G_0} \right) (T - 300) \right] \quad . \tag{2}$$

This model is largely a first order Taylor expansion in pressure and temperature, with a work hardening prefactor which is a power law in strain, ε. And we discuss briefly the Steinberg-Lund model, which is written as $\sigma = [\sigma_T + \sigma_A f(\varepsilon)]\, G/G_0$, where

$$\dot{\varepsilon} = \frac{1}{\frac{1}{C_1} \exp\left[\frac{2U_k}{kT} \left(1 - \frac{\sigma_T}{\sigma_P} \right)^2 \right] + \frac{C_2}{\sigma_T}} \tag{3}$$

Note, the Steinberg-Guinan model is independent of strain rate. The Steinberg-Lund model is strain-rate dependent, and in the phonon drag regime, gives a linear dependence of strength on strain rate. The PTW is also strain rate dependent, but in the phonon drag regime, strength increases roughly as strain rate to the ~1/4 power. These two material strength models differ significantly in their prediction of critical strain rate at which the deformation transitions from thermal activation to phonon drag. Once in the phonon drag regime, the Steinberg-Lund model assumes strength, σ, varies linearly with strain rate, $\sigma \sim d\varepsilon/dt$, whereas PTW assumes strength increases as $\sigma \sim (d\varepsilon/dt)^{1/4}$.

II. VANADIUM RAYLEIGH-TAYLOR EXPERIMENT

A typical target in our experiment has a "reservoir" consisting of 40 μm thick polyimide, $C_{22}H_{10}N_2O_5$ at density ρ = 1.42 g/cm^3, 125 μm thick polycarbonate, C_4H_4O at ρ = 1.2 g/cm^3, and 35 μm thick brominated polystyrene, $C_{50}H_{48}Br_2$ at ρ = 1.22 g/cm^3, glued together. This is followed by a 300 μm vacuum gap, then the rippled V sample. To thermally insulate the rippled V sample from the heat created by the stagnating plasma, we use a 7-8 μm thick, CH-based epoxy (Hardman Green) "heat shield", $C_{38}H_{53}N_1O_8$ at ρ = 1.14 g/cm^3, conformal on the ripple side and machined flat on the gap side. The rippled V sample is made by sputtering V onto a mandrel that has sinusoidal ripples of 60 μm wavelength and 0.6 μm amplitude machined onto its surface. The back surface of the V is polished flat, then the mandrel is chemically removed. The vanadium samples were full density, had an average grain size of ~ 1 μm in the lateral direction, 3-5 μm in the thickness (columnar) direction, and a measured tensile strength at ambient pressure and low strain rate of 7.15 kbar.[19] The drive calibration shots replaced the rippled V package with 10 μm Al backed by a 500 μm LiF window for interface velocity measurements.

We use six azimuthally symmetric laser beams at the Omega Laser, University of Rochester, each with E_L~135 J energy at laser wavelength of l_L=351 nm and 3.7 ns square pulse shape, to generate our drive. The ~640 μm diameter flat-top spatial profile is achieved using continuous phase plates (CPP) on the drive beams,[20] creating an average peak laser intensity of $I_L \sim 2.5 \times 10^{13}$ W/cm^2. This launches a strong shock through the reservoir which, at shock breakout, releases as a plasma across the 300 μm vacuum gap and stagnates first on the epoxy heat shield then the V sample, creating a ~1 Mbar ramped pressure in front of the V sample, as illustrated schematically in Fig.1a.[3,4] Based on Newton's second law, $P \sim \rho g z$, this causes the z =35 μm thick V sample to accelerate at a peak value of g ~ 5 x 10^{13} cm/s^2 (0.5 μm/ns^2). The accelerating sample is RT unstable; the ripples will tend to grow. When the material has strength, the RT growth rate can be considerably reduced compared to that of classical growth, i.e. the no strength case. This is clearly illustrated in the material density plots from 2D simulations at a sequence of times, shown in Fig. 1b. The sample is predicted to stay factors of 3-5 below the calculated melt temperature, using the Lindemann melt law.[15,16]

To measure the RT ripple growth, we use face-on radiography with a 5.2 keV laser driven vanadium He-α x-ray backlighter. For area backlighting, we use a large area x-ray source and a gated x-ray camera with a 2 x 2 array of 15 μm pinholes configured at magnification of ~6.[21] Alternatively, we use a ~15 μm diameter pinhole aperture placed just in front of the V backlighter foil to create a point source for projection imaging at magnification of ~19, onto a gated x-ray camera. Figure 2 on the right hand side shows example radiographs recorded at 40 and 80 ns. The contrast (light and dark bands or strips) are due to variations in transmitted backlighter x-ray intensity, $I = I_0 \exp(-z/\lambda_{mfp})$, where λ_{mfp} is the x-ray mean free path length, and z is the vanadium foil thickness. The RT growth causes foil thickness modulations of increasing depth, Δz, which cause x-ray optical depth modulations, $\Delta OD = \Delta z/\lambda_{mfp}$. Figure 2 (left hand side) shows lineouts of radiographic images of the ripples averaged over a 120 μm vertical window at delay times of 40 ns and 80 ns relative to the start of the drive laser, compared with fits using $\ln(I_v/I) = a \cdot \sin(\frac{2\pi}{\lambda} - \varphi)$. Here I is the average intensity through the rippled foil, I_v is the intensity in the ripple valleys (brighter regions), and a, λ and φ are the fitted amplitude, wavelength and the phase of the ripple. The perturbation growth is written as a growth factor, $GF(t) = \Delta OD(t)/(\Delta OD_0 \cdot MTF)$, where $\Delta OD(t)$ is the modulation in optical depth at time *t* due to the ripple, $\Delta OD_0 = \eta_0/\lambda_{mfp}$ is the initial optical depth, where $\lambda_{mfp} \sim 19.6$ μm is the mean free path length of the 5.2 keV backlighter x rays in vanadium. The optical depth calibration is quantified by step-wedge measurements. The $\Delta OD(t)$ is determined from the radiograph by a Fourier analysis of the ripple lineouts. The modulation transfer function (MTF), which quantifies the diagnostic spatial resolution, is measured on separate shots using a resolution grid: MTF > 0.8 for the $\lambda = 60$ μm ripples used in this experiment.

While there are a few analytical models of RTI perturbation growth calculations,[9] in order to include a complete hydrodynamic effects, our RT growth factor results are compared to the results from 2D radiation-hydrodynamics simulations including a constitutive strength model. After normalizing to the laser energy of 820 J, the self-consistent data set of *GF(t)* spanning several shot campaigns is shown by the red square symbols in Fig. 3. Typical experimental errors are estimated to be *dGF/GF* ~15% or less. We estimate an average strain rate, $\dot{\varepsilon}_{av}$ ~3 x 10^7 s^{-1}, by fitting a linear slope to the calculated strain over the interval of 25-40

ns. For t > 40 ns, this drops to $\dot{\varepsilon}_{av}$ ~ 3 x 10^6 s^{-1}. The top curve corresponds to a 2D simulation of the RT growth assuming no strength, and overpredicts the experimental data at 70 ns by a factor of ~6. Simulations using the PTW model using the as-published the default input parameters is the next highest curve; which also considerably over-predicts the experimental data. To fit our experimental data with the PTW model in Fig. 3, we lowered the critical strain rate for the transition from the thermal activation to the phonon drag regime from the default value of $\gamma\dot{\xi}$ ~10^9 s^{-1} to ~10^6 s^{-1}, accomplished by multiplying the PTW input parameters γ, y_0, and s_0 by 1/800, 0.60, and 0.68, respectively.[10,14] The default PTW parameters for V in the high-$\dot{\varepsilon}$ regime were set by overdriven shock experiments in Ta, also a BCC metal.[14] Furthermore, the strain rate interval of 10^4-10^9 s^{-1} was not modeled but rather "filled in" with PTW, due to the absence of reliable data to fit. So, it is not surprising that substantial changes in these input parameters for ramp loaded V were required. These changes to the PTW input parameters leave the strength predictions at $\dot{\varepsilon}$ < 10^6 s^{-1} (thermal activation regime) largely unchanged, while increasing the strength for $\dot{\varepsilon}$ > 10^6 s^{-1} (phonon drag regime). It is interesting to note that the Steinberg-Lund strength model,[13] which has several features similar to the PTW model, predicts the transition from thermal activation to phonon drag in vanadium would occur at $\dot{\varepsilon}_{crit}$~10^5 s^{-1} for default input parameters. Hence, the critical strain rate for the transition from thermal activation to phonon drag is uncertain by factors of 10^3-10^4, due to the lack of data in this ultrahigh-$\dot{\varepsilon}$ regime. The maximum strength occurs at the time of peak pressure and strain rate. The calculated peak strength for our RT experiments, σ_{max}~25 kbar, corresponds to a peak pressure and strain rate of 900 kbar and 3 x 10^7 s^{-1}. This is a factor of 3.5 higher than the measured ambient strength of 7.15 kbar.[19] Recent theoretical work shows that the shear modulus is not expected to increase significantly with pressure in this pressure range.[22] This suggests that our observed strength increase is due to rate effects rather than pressure. We estimate an overall ~20% uncertainty in our σ_{max}~25 kbar peak strength result, based on 10% due to the uncertainties in the growth factor measurements, 10% due to the uncertainties in our plasma drive, and 10% due to any potential model dependence in our analysis, all added in quadrature. During this extended series of V-RT shots, we also did shots where the peak pressure varied from 770 kbar to 950 kbar. For each shot, we inferred a peak strength by the methods describe above. Both models give peak strength increasing with peak pressure, but more importantly, both models give the same peak strength. So independent of which strength model we use, once the settings in the model have been adjusted to reproduce the RT experiment, they give the same predicted peak strength (corresponding to peak pressure). This suggests our experiments are more than just a test of strength models at high pressures and strain rates, but a means of inferring peak strength itself, albeit indirectly.

III. DISCUSSION

We now compare to an analytic RT growth model that treats strength as an effective lattice viscosity. In the linear regime, classical RT growth can be written as $GF \approx e^{\int \gamma_{classical} dt}$, where $\gamma_{classical} \approx [A \cdot \frac{2\pi}{\lambda} \cdot g(t)]^{1/2}$ gives the growth rate for inviscid fluids, and *A*, λ, and *g* are the Atwood number, perturbation wavelength, and foil acceleration, respectively. For viscous fluids, the RT growth rate is determined from $\gamma_{RT}^2 + 2k^2\nu\gamma_{RT} - gkA = 0$, where $\nu(cm^2/s) = \mu/\rho$ is the kinematic viscosity, μ(dyne·sec/cm^2=poise) is the dynamic (absolute) viscosity, and ρ is

material density.[23,24] We show these analytic results for RT growth factors versus perturbation wavelength at 70 ns in Fig. 4. Experimental data were taken at $\lambda = 40$ and 60 μm (red squares). The 2D simulations were done at λ = 40, 60, and 100 μm with the modified strength models (blue diamonds, green triangles), and with strength turned off (black circles). The smooth curves in Fig. 4 correspond to (in order from the top) dynamic viscosities of 0, 100, 200, 400, and 800 poise, with a best fit at ~400 poise We show also in Fig. 3 the growth factor time evolution for the viscous model using 400 poise. As a consistency check, we use a relationship equating strength with an effective lattice viscosity,[24] $\nu = \mu / \rho \approx \sigma /(\sqrt{6}\rho\langle\dot{\varepsilon}\rangle)$, giving $\sigma \approx \sqrt{6}\langle\dot{\varepsilon}\rangle\mu$. Using an average strain rate of $\langle\dot{\varepsilon}\rangle \approx 3 \times 10^7$ s^{-1} over the interval of 25-40 ns from the 1D radiation-hydrodynamics simulations and the fitted viscosity of 400 poise gives an estimated peak strength of σ_{max}~29 kbar. For a second estimate, we make a rough approximation of strain rate from $\langle\dot{\varepsilon}\rangle \approx \frac{1}{3}\dot{\rho}/\rho \approx \frac{1}{3}(\Delta\rho/\rho_0)/\Delta t_{rise.time}$. The equation of state of V,[25] allows an estimate of compression at $\rho/\rho_0 \sim 1.4$, which occurs over the measured rise time of ~6 ns, giving $\langle\dot{\varepsilon}\rangle \approx 2 \times 10^7$ s^{-1}. This gives a second estimate of peak strength of σ_{max}~19 kbar. These two analytic approximations bracket the more accurate result for the strength at peak pressure of σ_{max}~25 kbar inferred from the 2D RT simulations.

We also compare our results of the RT growth using a new multiscale material model for vanadium[26] and the simulation results are shown in Fig. 5. This model starts with an interatomic potential with a form derived from quantum mechanics and parameterized by first-principles calculations.[22] This interatomic potential is then incorporated into molecular dynamics (MD) simulations, to calculate the dynamic properties of individual dislocations, such as their velocity as a function of applied shear stress and lattice temperature. The dynamics of individual dislocations are parameterized, then input into dislocation dynamics simulations, to calculate the dislocation density evolution, work hardening, and strength as a function of the relevant parameters such as lattice pressure, temperature, strain, and strain rate. Finally, these results are parameterized, and incorporated into the continuum code, ALE3D to calculate the actual RT instability evolution in the experiment. For the results shown in Fig. 5, the same plasma drive as discussed above was used. This multiscale simulation, without adjusting any parameters, overpredicts the experimental RT growth by 40-50%. As shown in Fig. 5, all of the fundamental parameters, such as dislocation velocity, dislocation density, and strain rate are contained in this simulation. Also evident is a variation in strain rate and temperature across the ripple.

Our inferred macroscopic fluid viscosity of ~400 poise can be used to derive an order of magnitude estimate of the microscopic dislocation drag coefficient in the phonon drag regime at these very high strain rates. Based on the definition of (macroscopic) viscosity, we write

$$\sigma_{shear} = \frac{\mu_{viscosity} v_{RT}^{bubble}}{\lambda_{RT}/2} = \mu_{viscosity}\dot{\varepsilon} \qquad (4)$$

where μ is the dynamic viscosity, σ_{shear} is the shear stress driving the RT instability, v_{RT} is the RT bubble velocity for perturbation of wavelength λ_{RT}, and $\dot{\varepsilon}$ is the resulting RT-induced strain rate. At the lattice level, the applied shear stress is related to terminal dislocation velocity by,[27]

$\sigma_{shear} b = MBv_{disloc}$, where *b* is the Burgers vector, *M* is the Taylor factor that relates the applied shear stress to an average resolved shear stress for the operative slip planes for polycrystalline samples, *B* is the dislocation drag coefficient, and v_{disloc} is the average dislocation velocity.[28] The Taylor analysis results in one factor of M for the stress and a second for the strain (and strain rate), as verified in low rate experiments.[29] Orowan's equation relates macroscopic strain rate to the microscopic parameters, $\dot{\varepsilon} = \rho_{\mathrm{disloc}} b v_{\mathrm{disloc}} / \mathrm{M}$, where ρ_{disloc} is the dislocation density. These equations can be combined to give

$$\frac{\mu_{viscosity}}{B_{drag}} = \frac{M^2}{\rho_{disloc} b^2} \qquad (5)$$

Taking $\mu_{viscosity} \sim$ 400 Poise, a dislocation density of 2 x 10^{11} cm^{-2} from a multi-scale simulation of our RT experiment (see Fig. 5) at peak pressure,[26] b_0 ~ 3 Angstroms, $b = b_0/(\rho/\rho_0)^{1/3}$ under compression of $\rho/\rho_0 = 1.4$, and *M* = 2.889 (for our textured vanadium sample[38]) gives *B* ~ 10^{-2} dyne·s/cm^2. We have thus inferred a dislocation drag coefficient of ~0.01 dyne·s/cm^2 in the phonon drag regime under the peak pressure (~1 Mbar) and very high strain rate (~10^7 s^{-1}) conditions in our vanadium RT experiment. This inferred phonon drag coefficient is consistent with that quoted by Nemaat-Nasser.[30]

Acknowledgement: This work was performed under the auspices of the Lawrence Livermore National Laboratory under Contract No. DE-AC52-07NA27344.

REFERENCES

[1]B. A. Remington et al., Materials Science and Technology 22, 474 (2006).
[2]P. W. Bridgman, *Collected Experimental Papers* (Harvard University Press, Cambridge, 1964).
[3]J. Edwards et al., Phy. Rev. Let. 92, 075002 (2004).
[4]K.T. Lorenz, M. J. Edwards, A. F. Jankowski, S. M. Pollaine, R. F. Smith, and B. A. Remington, High Energy Density Physics 2, 113 (2006).
[5]Lord Rayleigh, Phil. Mag. 34, 145 (1892).
[6]G. Taylor, Proc. R. Soc. A 201, 192 (1950).
[7]D. H. Sharp, Physica D 12, 3 (1984).
[8]J. F. Barnes, P. J. Blewett, R. G. McQueen, K. A. Meyer, and D. Vernable, J. Appl. Phys. 45, 727 (1974).
[9]A. R. Piriz, J. J. López Cela, and N. A. Tahir, Phys Rev. E, 80, 046305 (2009).
[10]Hye-Sook Park et al., Phys. Rev. Lett., in press (March, 2010).
[11]Marc A. Meyers, *Dynamic Behavior of Materials* (John Wiley & Sons, Hoboken, NJ, 1994).
[12]G. Regazzoni, U.F. Kocks, and P.S. Follansbee, Acta Metall. 35, 2865 (1987).
[13]D. J. Steinberg and C. M. Lund, J. Appl. Phys. 65, 1528 (1989).
[14]D. L. Preston, D. L. Tonks, and D. C. Wallace, J. Appl. Phys. 93, 211 (2003).
[15]David A. Young, *Phase Diagrams of the Elements* (Univ. of Calif. Pres, Berkeley (1991).
[16]D.J. Steinberg, S.G. Cochran, and M.W. Guinan, J. Appl. Phys. 51, 1498 (1980).
[17]B.A. Remington et al., in Shock Compression of Condensed Matter – 2005, edited by M.D. Furnish, M. Elert, T.P. Russell, and C.T. White (AIP, 2006), p. 765.

[18]B. A. Remington et al., "Developing an experimental test bed for strength models at ultrahigh pressures", submitted to High Energy Density Physics (2009).
[19]A.F. Jankowski, J. Go, and J.P. Hayes, Surface & Coatings Tech. 202, 957 (2007).
[20]C. A. Haynam et al., Appl. Optics 46, 3276 (2007).
[21]K. T. Lorenz, M. J. Edwards, S. G. Glendinning, A. F. Jankowski, J. McNaney, S. Pollaine, and B. A. Remington, Phys. Plasmas **12**, 056309 (2005)
[22]R. E. Rudd and J. E. Klepeis, J. Appl. Phys. 104, 093528 (2008).
[23]K. O. Mikaelian, Phys. Rev. E 47, 375 (1993).
[24]J.D. Colvin et al., J. Appl. Phys. 93, 5287 (2003).
[25]*High-Velocity Impact Phenomena*, Ed. Ray Kinslow (Academic Press, New York, 1970).
[26]R. Becker, A. Arsenlis, J. Marian, M. Rhee, M. Tang, and L. Yang, See National Technical Information Service Document No. DE2009964080 ("Continuum level formulation and implementation of a multi-scale model for vanadium"). Aug. (2009). Copies may be ordered from the National Technical Information Service, Springfield VA 22161
[27]R. Kapoor and S. Nemat-Nasser, Met. Mat. Trans. A, 35A, 815 (2000).
[28]M.A. Meyers and K.K. Chawla, *Mechanical Metallurgy: Principles and Applications* (Prentice-Hall, 1984).
[29]G. I. Taylor, J. Inst. Metals 62, 307 (1938).
[30]S. Nemat-Nasser and W. Guo, Mechanics of Materials 32, 243 (2000).

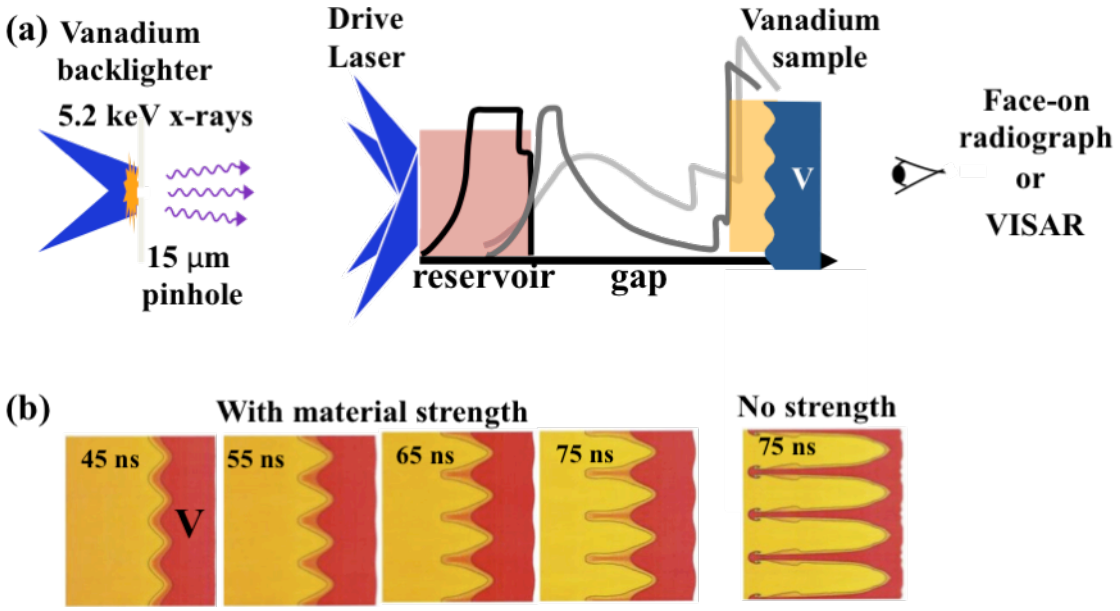

Figure 1. (a) Schematic illustrating the experimental configuration. (b) Density plots of the RT growth from simulations at 45, 55, 65, and 75 ns, using the PTW strength model with input parameters modified to reproduce the RT data shown in Fig. 3. The second plot at 75 ns (far right hand side) is for no strength, showing the much greater RT growth.

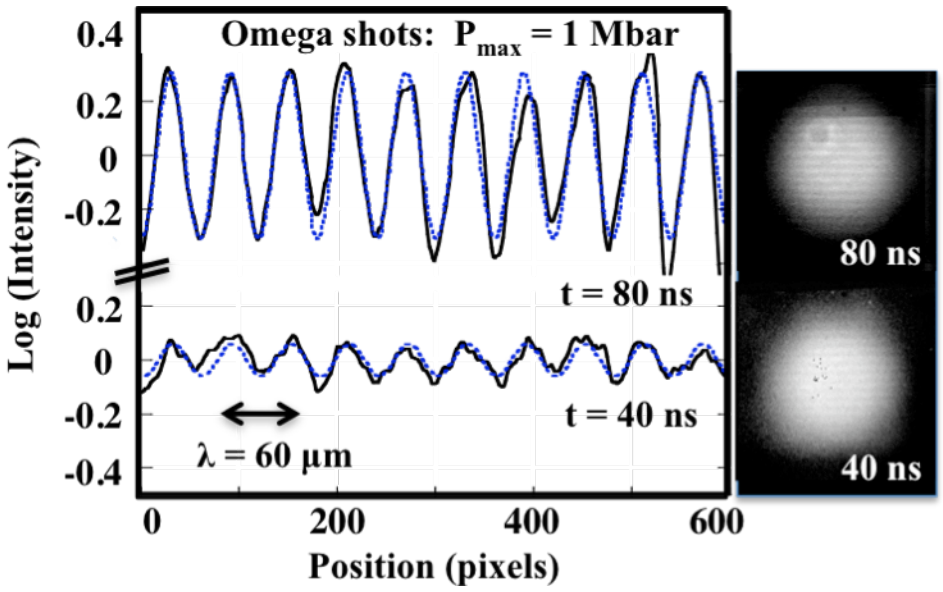

Figure 2. Results from the in-flight x-ray radiographs of the driven V-RT samples. On the right hand side are example x-ray radiographs taken at 40 and 80 ns. On the left hand side are lineouts of log(intensity) averaged over 120 μm. The smooth curves are fitted with single-mode sinusoids with a wavelength of $\lambda = 60\ \mu m$, adjusting only the amplitude.

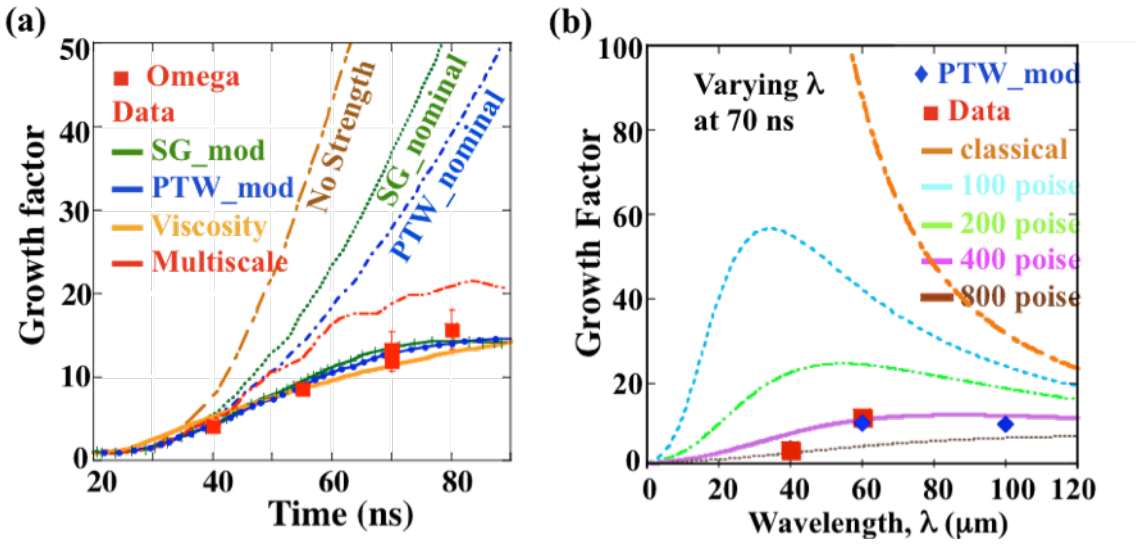

Figure 3. (a) Measured and simulated Rayleigh-Taylor (RT) growth of the pre-imposed ripple in the driven vanadium foil. The solid red square plotting symbols give the experimental data. The smooth curves correspond to the simulations. (b) Measured versus analytic RT dispersion curves, given as growth factor vs. perturbation wavelength at a time of 70 ns. The blue diamond solid plotting symbols correspond to a simulation with the PTW strength model adjusted to fit the experiment. The square red plotting symbols at λ = 40 μm and 60 μm correspond to the experimental measurements. The smooth curves correspond to the analytic viscous RT model assuming viscosities of (from the top) 0, 100, 200, 400, and 800 poise.

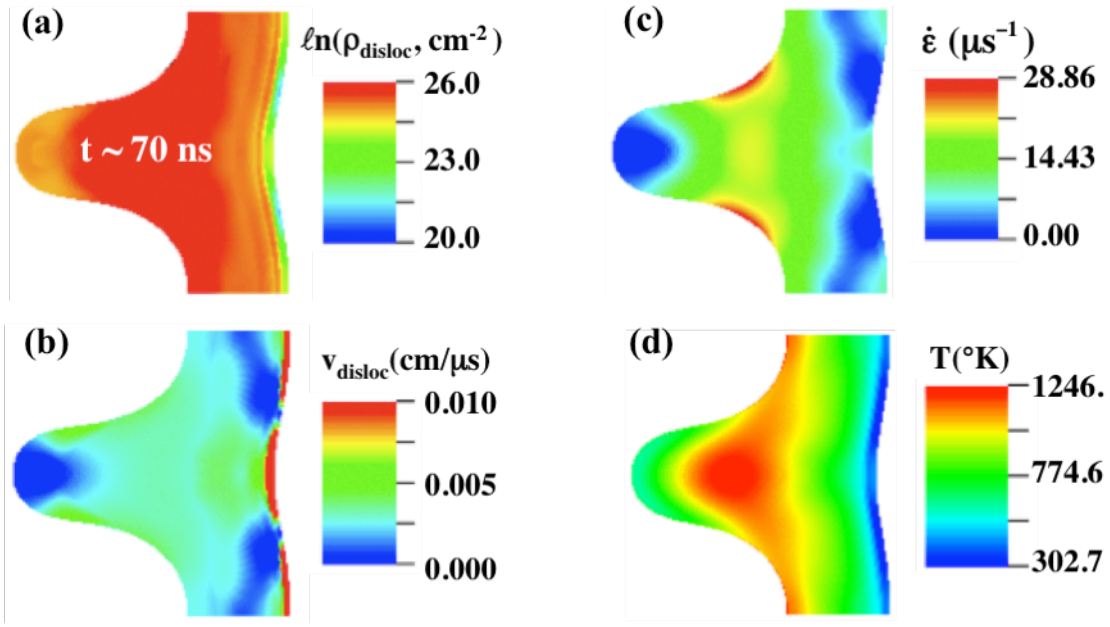

Figure 4. Results from a simulation of this V-RT experiment using a multiscale material model. The vanadium sample ripple amplitude and shape from the simulation at t = 70 ns is shown. are the V-RT ripple from the simulation at t ~ 70 ns. The color scale gives (a) the natural log of the screw dislocation density in cm^{-2}, (b) the screw dislocation velocity in cm/μs, (c) strain rate in μs^{-1}, and (d) sample temperature (K).